Transition between Positive and Negative Hexagons in Optical Pattern Formation

T. Ackemann, Yu. A. Logvin,* A. Heuer, and W. Lange
Institut für Angewandte Physik, Westfälische Wilhelms-Universität Münster, Corrensstraße 2/4, D-48149 Münster, Federal Republic of Germany
(Received 2 June 1995)

We report the observation of the transition between positive and negative hexagons by using optical pattern formation in a sodium vapor cell with a feedback mirror. We show that because of a secondary instability of a developed hexagon against its spatial ultraharmonics a new pattern (ultrahexagon) appears. Pattern formation for an incident Gaussian light beam takes place in combination with switching effects that result in flowerlike structures. The data from analytical investigations and numerical simulations based on a microscopic theory are in good accordance with experiment.

PACS numbers: 42.65.–k, 42.50.Ne, 47.54.+r

Hexagonal structures are generic just above threshold in pattern-forming systems when a quadratic term governs the equation for the order parameter [1,2]. Depending on its sign, hexagons exist in two (complementary) forms: positive or $H0$ hexagons, which are hexagonally arranged peaks (maxima of amplitude) on a background, and negative or $H\pi$ hexagons (also called honeycombs), which are dips (amplitude minima) in the background. When spatial instabilities occur only in a finite interval of a control parameter, the sign of the quadratic nonlinear term—and thus the type of hexagonal structure—can be different on the opposite ends of the interval [3]. Examples of $H0$- and $H\pi$-hexagon coexistence, obtained in the framework of the Swift-Hohenberg equation [4], shed some light on experiments in Rayleigh-Bénard convection [5] and in reaction-diffusion systems [6]. The situation appears to be far from clear mostly because of the fact that a comparison of experimental results with a realistic theoretical model is lacking.

Using a nonlinear medium with a single feedback mirror proved to be fruitful in studies of optical pattern formation [7–13]. For a Kerr-like medium [8–11] hexagons are observed, but they are of one type only, unless the intrinsic symmetries are disturbed by introducing nonlocal and nonhomogeneous elements in the feedback [11]. The purpose of this Letter is to study experimentally and theoretically the metamorphoses of structures by replacing the Kerr-like medium by an atomic vapor under suitably chosen conditions.

The system under study consists of a sodium vapor cell with length l and feedback mirror (d is the distance between the cell and the mirror) in an external magnetic field B. The cell is irradiated by circularly polarized light with amplitude E_0 (Fig. 1). The field transmitted through the cell $E_t = E_0 e^{-i\chi kl/2}$ (χ is the susceptibility of the sodium vapor) is transformed after propagation in free space and reflection from the mirror into $E_b = \sqrt{R}\,\hat{W}E_t$. Here $\hat{W}$ is the linear propagation operator whose explicit form is determined by the paraxial wave equation and R is the reflection coefficient of the mirror. Neglecting diffraction and standing wave effects—the corresponding grating has a period of only 300 nm in our case and will be washed out by atomic diffusion—inside the nonlinear medium in the manner of Ref. [8], we assume the total intensity in the cell to be $I = |E_0|^2 + |E_b|^2$.

Under our experimental conditions, the origin of the nonlinearity of the medium is optical pumping, e.g., the creation of a population difference (or orientation) between sublevels of the sodium ground state. In a formal description the equation of motion for the Bloch vector $\mathbf{m} = (u, v, w)$ [14,15]

$$\partial_t \mathbf{m} = -(P - D\Delta_\perp + \gamma)\mathbf{m} - \mathbf{m} \times \mathbf{\Omega} + \hat{\mathbf{e}}_z P \quad (1)$$

has to be considered. Here $P = I|\mu_e|^2/4\hbar^2\Gamma_2(\overline{\Delta}^2 + 1)$ (Γ_2 denotes the relaxation rate of the optical coherence and $\overline{\Delta}$ the detuning between the incident field and the atomic transition, normalized to Γ_2) can be interpreted as the optical pump rate, D is the diffusion constant, $\Delta_\perp$ is the transverse part of the Laplacian, $\mathbf{\Omega} = (\Omega_x, 0, \Omega_z - \overline{\Delta}P)$ is an effective Larmor frequency vector [15], and γ is a small parameter which simulates decay processes through collisions with the buffer gas atoms. Equation (1) is derived by treating the sodium D_1 line as a homogeneously broadened $J = 1/2 \rightarrow J' = 1/2$ transition. This approximation is found to be very useful, if the experiment is performed in a high pressure buffer gas atmosphere [14]. Calculating from Eq. (1) the orientation $w = m_z$ and inserting it into the expression for

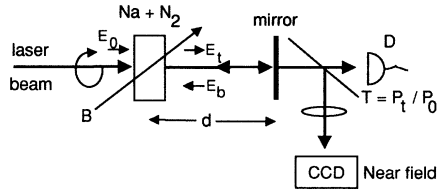

FIG. 1. Scheme of the experiment. See text.

 0031-9007/95/75(19)/3450(4)$06.00

the susceptibility

$$\chi = -\frac{N|\mu_e|^2}{2\hbar\epsilon_0\Gamma_2}\frac{\bar{\Delta} + i}{\bar{\Delta}^2 + 1}(1 - w) \equiv \chi_{\text{lin}}(1 - w), \quad (2)$$

where N is the sodium particle density, we couple the equations for field and medium.

Referring to the pump rate P_0 introduced by the forward beam ($P_0 \sim |E_0|^2$) as a control parameter, we find the steady-state plane-wave solution for the orientation w_s from the algebraic equation

$$w_s = \frac{P_s}{\gamma + P_s}\frac{(\Omega_z - \bar{\Delta}P_s)^2 + (\gamma + P_s)^2}{(\Omega_z - \bar{\Delta}P_s)^2 + (\gamma + P_s)^2 + \Omega_x^2}, \quad (3)$$

with $P_s = P_0(1 + R|e^{[-ikl\chi_{\text{lin}}(1-w_s)/2]}|^2)$. Equation (3) is a nonlinear equation in respect to w_s that can provide bistable behavior of the characteristic $w_s(P_0)$ as shown in Fig. 2(a). At first, for small P_0, w_s increases very quickly from zero because of saturation of the first factor in Eq. (3) (small parameter γ), then it decreases under the action of the second factor up to the bistable region and then it increases again [16]. This shape of $w_s(P_0)$, due to the relation between w_s and the refractive index $n = 1 + \text{Re}(\chi_{\text{lin}})(1 - w_s)/2$, determines the nonlinear medium for negative detuning $\bar{\Delta}$ to be self-defocusing on the intervals with positive slope, but self-focusing when w_s decreases with P_0.

Stability analysis in respect to a spatial inhomogeneous perturbation proportional to $\cos(k_\perp r_\perp)$ yields in the first order of perturbation theory the marginal stability condition that permits one to find unstable domains on the steady-state characteristic in Fig. 2(a). Because of the self-focusing property of the medium on the interval with negative slope, the structures created here have a different, namely, larger, spatial period than the patterns on the increasing, self-defocusing, part of the characteristic in accordance with the predictions of Kerr-medium theory [8]. For the set of parameters of Fig. 2 the bands of possible spatial periods Λ are [0.45 mm; 1.50 mm] for self-focusing and [0.28 mm; 0.37 mm] for the self-defocusing case.

Assuming a perturbation in the form of a hexagonal mode, we have investigated the vicinity of the bifurcation points in the second order of perturbation theory [17]. The result is that $H\pi$ hexagons should exist close to points A and D, but $H0$ ones at points B and C.

In numerical simulations we used the explicit difference scheme to integrate Eq. (1) and the fast Fourier transform to propagate the light field in free space between the mirror and the medium. Periodic boundary conditions have been imposed to check the analytical results of the plane-wave approach and Dirichlet ones ($\mathbf{m}|_\Sigma = 0$) to simulate the real experiment where the magnetization vanishes at the cell walls.

In the case of the plane-wave treatment, in accordance with the stability analysis, simulations show the appearance of $H\pi$ hexagons above the threshold in point A in Fig. 2(a) (length scale $\Lambda \approx 0.55$ mm). With increasing pumping they become unstable and lead to the development of irregular spatiotemporal behavior with strong similarity to defect-mediated turbulence. Close to point B positive hexagons arise from the turbulent state. Their length scale $\Lambda = 0.41$ mm indicates that they are not ordinary primary structures predicted by the stability analysis. Closer inspection with the help of simulations reveals that in the vicinity of the point B ordinary $H0$ hexagons, which develop from the homogeneous state and have here a spatial period $\Lambda \approx 0.7$ mm, are unstable against their spatial ultraharmonics. As the resulting pattern we observe here a branch of ultrahexagons (UH0) with a length scale smaller than the primary hexagon size by a factor $\sqrt{3}$. This metamorphosis is illustrated in Fig. 2(b) in which the amplitudes of hexagons found from numerical simulations are presented. One can see that primary hexagons evolve to the turbulent state if the branch of

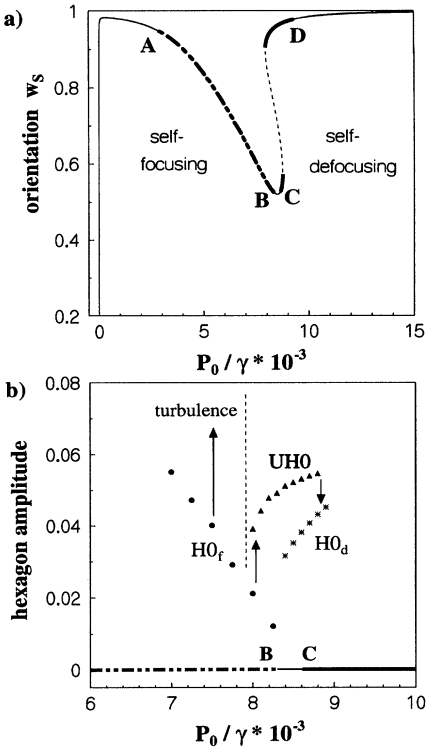

FIG. 2. (a) Steady-state orientation w_s versus external pumping. Pattern formation intervals are marked by the thick lines. The dashed line indicates the unstable branch in the region of bistability. Parameters: $N = 1.2 \times 10^{14}$ cm^{-3}, $\bar{\Delta} = -8$, $R = 0.915$, $l = 15$ mm, $\Omega_x/2\pi = 9$ kHz, $\Omega_z/2\pi = -78$ kHz ($B_x = 1,3$ μT, $B_z = -11$ μT). (b) Amplitudes of unstable positive hexagons (circles), ultrahexagons (triangles), and self-defocusing positive hexagons (asterisks) in the vicinity of points B and C. The arrows illustrate the decay of the unstable hexagonal solution.

ultrahexagon solution does not exist. The reason for this secondary bifurcation to ultrahexagons lies in the rather sophisticated nonlinearity in the system ("beaklike" behavior of the steady-state characteristic). We note that the basic $H0$ hexagons are stable for other parameters for which the steady-state characteristic is less winding and has no bistable interval.

After the minimum of the steady-state characteristic, above point C, we find $H0$ hexagons of a different kind with a length scale $\Lambda = 0.34$ mm which belongs to a defocusing nonlinearity. (In simulations we have observed switching from the self-focusing ultrahexagons to the self-defocusing $H0_d$ hexagons.) For increasing intensity these self-defocusing hexagons also evolve towards a turbulent state, from which the system is switching to the upper steady-state branch beyond the bifurcation point D, where the system becomes stable against transverse perturbations due to strong saturation.

To check the theoretical predictions experimentally, a slightly modified version of the setup described in [13] is used (see Fig. 1). The enlarged beam ($w_0 = 1.38$ mm $1/e^2$ point of intensity) of a cw dye laser, tuned slightly below the D_1 resonance line of sodium, is injected into a cell of cylindrical cross section which contains sodium in a buffer gas atmosphere (300 hPa of nitrogen). Spatial filtering by a single-mode fiber ensures a smooth and nearly Gaussian intensity profile and cylindrical symmetry (astigmatism $<1\%$) of the incoming beam. The length of the interaction region in the cell is 15 mm, which is 1 order of magnitude less than the free space propagation length to the feedback mirror ($d = 175$ mm). The exit face of the medium is imaged onto a CCD camera. A fraction of the transmitted beam is focused on a detector for a measurement of the space-integrated transmission of the cell.

If the power of the incident beam is scanned adiabatically, the transmission coefficient T displays the behavior shown in Fig. 3, which correlates very well with theoretical results based on Gaussian beam simulations. Above the threshold, a transverse pattern in the form of three dark holes appears [Fig. 4(a)]. Increasing the beam power results in the formation of a pattern with five holes in a pentagonal arrangement, which gives way to the blurred, nonstationary pattern in Fig. 4(b). From this, bright spots emerge. Again, the number of spots (three to seven) increases with power. Figure 4(c) shows the hexagonal state. After the minimum in the transmission curve, flowerlike patterns [Fig. 4(d)] with a plateau in the beam center are observed. The number of petals starts with seven and increases with pumping up to 14. The length scale of the pattern is basically independent from the number of peaks and is about 0.40 mm before and 0.33 mm after the minimum in the transmission curve. (The length scale was determined from the Fourier transform as well as by directly measuring the distance between neighboring peaks in the normal space.) We mention that the patterns

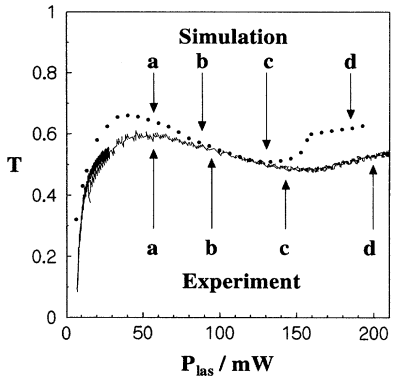

FIG. 3. Transmission coefficient: solid line—experiment, circles—simulation for incident Gaussian beam with $I_0(r) = 2P_{las}/\pi w_0^2 \exp(-2r^2/w_0^2)$, $w_0 = 1.38$ mm, $\gamma = 6\ s^{-1}$, and other parameters as in Fig. 2. The power scaling of the simulation was corrected by a factor of 3/16 to take into account the hyperfine structure of sodium [15].

with peaks on an annulus [like the ones in Fig. 4(c) and 4(d)] have the tendency to rotate if the feedback mirror is only slightly misaligned. In some cases the rotation of the patterns cannot be stopped by mirror alignment. The hexagon in Fig. 4(c), e.g., is only a snapshot (but it can be observed as stable for other parameters). Whether this is due to a small residual misalignment (resolution ≈ 0.1 mrad) or an intrinsic instability is open at this point of investigations.

One can see from Fig. 4 that all kinds of patterns—including the length scales—are reproduced in simulations. It is obvious, however, that the patterns are greatly affected by the limited beam size, which is especially important for the dark hole patterns [Fig. 4(a)] since they have the largest length scale. The observed selection of a structure with dihedral symmetry in a situation in which the hexagonal structure is hindered by the boundary conditions is in agreement with previous theoretical and experimental studies of the single-mirror feedback system [10,13]. Experiments with a larger aspect ratio (smaller distance $d = 75$ mm) show that a hexagonal lattice of dark holes is indeed the generic one at the beginning of the part of the transmission curve with negative slope. Figure 4(e) shows a typical example. However, for the parameters, where these distinct negative hexagons are observed, the available laser beam power is not sufficient to reach the opposite end of the instability interval.

In addition to the finite extent of the beam, the Gaussian profile imposes further constraints, since the power level for a certain kind of pattern is only satisfied in an annulus. A consequence of the latter can be seen very nicely in the pattern of Fig. 4(d), where in the center no transverse patterns occur [operation interval right to point D in Fig. 2(a)]. The petals correspond to the $H0_d$ hexagons (after point C), whereas in the wings of the beam with

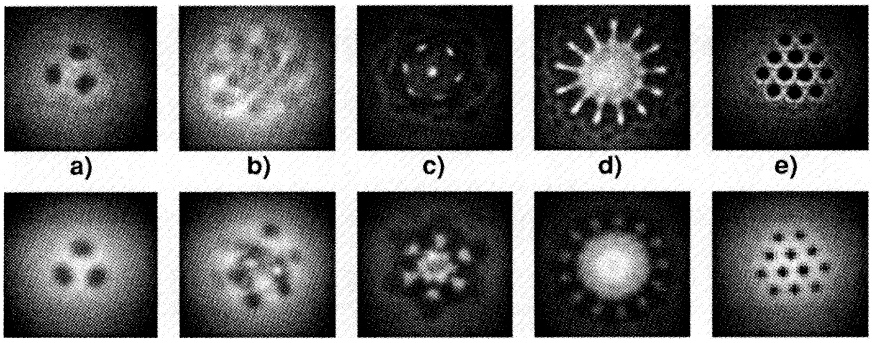

FIG. 4. Experimental (top) and corresponding simulated (bottom) patterns in the points (a)–(d) marked in Fig. 3. (e)—well developed pattern illustrating $H\pi$ hexagons for parameters: $N = 1.1 \times 10^{14}$ cm^{-3}, $\bar{\Delta} = -8.2$, $\Omega_x/2\pi = 41$ kHz, $\Omega_z/2\pi = -260$ kHz ($B_x = 5.9$ μT, $B_z = -37.2$ μT), $P_{\text{las}} = 138$ mW. The frames have a size of 2.5 mm $\times$ 2.5 mm.

low intensity dark holes are still visible. Let us recall that the number of petals might be odd [e.g., 13 in Fig. 4(d)] and that far and near fields are different. Therefore it is clear that they cannot be interpreted as Gauss-Laguerre modes as in the experiment of Grynberg and co-workers in rubidium vapor [12,18]. In contrast, the observation of a characteristic length of 0.33 mm in a substantial region of input power seems to indicate that the system adjusts the number of petals to the diameter of the saturated central region, while keeping the distance between the petals constant. Thus we identify the petals to be the remnants of the $H0_d$ hexagons found in the plane wave theory. In the same manner, the observed length scale of 0.4 mm for the patterns with peaks before the minimum in the transmission curve indicate that they originate from the ultrahexagons.

In conclusion, we have first shown both theoretically and experimentally that the negative hexagons and positive ultrahexagons emerge on the opposite ends of a instability interval. For the case of our experimental parameters, the hexagonal patterns are conjugated through a turbulent state, but the search for a different scenario is continued.

We thank F. Mitschke for much advice in preparing the fiber-optical system. Yu. A. L. was supported by the Deutscher Akademischer Austauschdienst.

*Permanent address: Institute of Physics, Belarusian Academy of Sciences, Skaryna ave. 70, 220072, Minsk, Belarus.

[1] F. H. Busse, J. Fluid Mech. **30**, 625 (1967).
[2] S. Ciliberto, P. Coullet, J. Lega, E. Pampaloni, and C. Perez-Garcia, Phys. Rev. Lett. **65**, 2370 (1990).
[3] W. J. Firth and A. J. Scroggie, Europhys. Lett. **26**, 521 (1994); M. Tlidi and P. Mandel, Chaos, Solitons and Fractals **4**, 1475 (1994).
[4] M'F. Hilali, S. Métens, P. Borckmans, and G. Dewel, Phys. Rev. E **51**, 2046 (1995); G. Dewel, S. Métens, M'F. Hilali, P. Borckmans, and C. B. Price, Phys. Rev. Lett. **74**, 4647 (1995).
[5] G. Ahlers, L. I. Berge, and D. S. Cannell, Phys. Rev. Lett. **70**, 2399 (1993); M. Assenheimer and V. Steinberg (private communication).
[6] Q. Ouyang and H. L. Swinney, Chaos **1**, 411 (1991).
[7] G. Giusfredi, J. F. Valley, R. Pon, G. Khitrova, and H. M. Gibbs, J. Opt. Soc. Am. B **5**, 1181 (1988).
[8] G. D'Alessandro and W. J. Firth, Phys. Rev. A **46**, 537 (1992).
[9] R. MacDonald and H. J. Eichler, Opt. Commun. **89**, 289 (1992); B. Thüring, R. Neubecker, and T. Tschudi, Opt. Commun. **102**, 111 (1993).
[10] F. Papoff, G. D'Alessandro, G.-L. Oppo, and W. J. Firth, Phys. Rev. A **48**, 634 (1993); E. Ciaramella, M. Tamburini, and E. Santamato, Phys. Rev. A **50**, R10 (1994).
[11] E. Pampaloni, S. Residori, and F. T. Arecchi, Europhys. Lett. **24**, 647 (1993).
[12] G. Grynberg, A. Maître, and A. Petrossian, Phys. Rev. Lett. **72**, 2379 (1994).
[13] T. Ackemann and W. Lange, Phys. Rev. A **50**, R4468 (1994).
[14] F. Mitschke, R. Deserno, W. Lange, and J. Mlynek, Phys. Rev. A **33**, 3219 (1986).
[15] M. Möller and W. Lange, Phys. Rev. A. **49**, 4161 (1994).
[16] A discussion of the physical origin of the behavior has to be postponed to a forthcoming paper.
[17] P. Manneville, *Dissipative Structures and Weak Turbulence* (Academic, Boston, 1990).
[18] In this experiment the linear input polarization introduces additional symmetry which cancel the quadratic nonlinearity and thus rules out the existence of hexagons as shown in A. J. Scroggie, Ph.D. thesis, Glasgow, 1995; M. Le Berre *et al.*, Opt. Commun. **118**, 447 (1995).

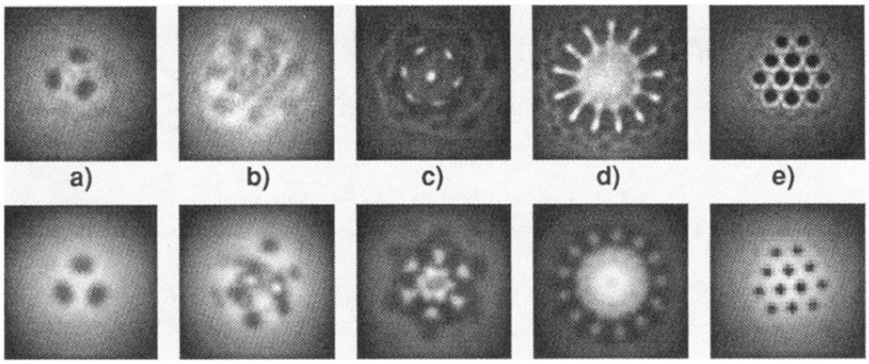

FIG. 4. Experimental (top) and corresponding simulated (bottom) patterns in the points (a)–(d) marked in Fig. 3. (e)—well developed pattern illustrating $H\pi$ hexagons for parameters: $N = 1.1 \times 10^{14}$ cm^{-3}, $\overline{\Delta} = -8.2$, $\Omega_x/2\pi = 41$ kHz, $\Omega_z/2\pi = -260$ kHz ($B_x = 5.9$ μT, $B_z = -37.2$ μT), $P_{\text{las}} = 138$ mW. The frames have a size of 2.5 mm $\times$ 2.5 mm.